Contributions of cell behavior to geometric order in embryonic cartilage

Sonja Mathias[1], Igor Adameyko[2,3†], Andreas Hellander[1†], Jochen Kursawe[4†]

[1]Department of Information Technology, Division of Scientific Computing, Uppsala University, Uppsala, Sweden
[2]Department of Physiology and Pharmacology, Karolinska Institutet, Solna, Sweden
[3]Department of Neuroimmunology, Center for Brain Research, Medical University of Vienna, Vienna, Austria
[4]School of Mathematics and Statistics, University of St Andrews, St Andrews, UK

June 27, 2022

† co-senior authors

Abstract

During early development, cartilage provides shape and stability to the embryo while serving as a blueprint for the skeleton. Correct formation of embryonic cartilage is hence essential for healthy development. In vertebrate cranial cartilage, it has been shown that a flat and laterally extended macroscopic geometry is linked to regular microscopic structure consisting of tightly packed, short, transversal clonar columns. However, it remains an ongoing challenge to identify how individual cells coordinate to successfully shape the tissue, and more precisely which mechanical interactions and cell behaviors contribute to the generation and maintenance of this columnar cartilage geometry during embryogenesis. Here, we apply a three-dimensional cell-based computational model to investigate mechanical principles contributing to column formation. The model accounts for clonal expansion, anisotropic proliferation and the geometrical arrangement of progenitor cells in space. We confirm that oriented cell divisions and repulsive mechanical interactions between cells are key drivers of column formation. In addition, the model suggests that column formation benefits from the spatial gaps created by the extracellular matrix in the initial configuration, and that column maintenance is facilitated by sequential proliferative phases. Our model thus correctly predicts the dependence of local order on division orientation and tissue thickness. The present study presents the first cell-based simulations of cell mechanics during cranial cartilage formation and we anticipate that it will be useful in future studies on the formation and growth of other cartilage geometries.

1 Introduction

Correct formation of embryonic cartilage is essential for healthy development. Cartilage provides structural support to the growing embryo and it serves as precursor to bone formation. A recent study investigating the cellular structure of cartilage in mouse embryos revealed that embryonic cartilage is highly geometrically ordered [1].

For example, cells inside growth plates of the cartilaginous skull are arranged in columns. These columns are oriented transversally and arranged adjacent to each other in the lateral direction. The columns emerge from an initial, disordered, mesenchymal condensation. Once a thin, ordered sheet with a column length of 4-6 chondrocytes is formed, the sheet thickens as columns increase in length, and lateral growth relies on the insertion of new columns [1]. This insertion of new columns starts from the perichondrial stem-like cell layers on the tissue

boundaries such that cells in one column typically are daughters of one perichondrial cell. Ordered spatial cell arrangement was also reported in other embryonic cartilage structures, such as rod-like structures that precede the formation of long bones [1].

What mechanisms contribute to this high level of geometric order? Kaucka et al showed that column formation relies on oriented cell division, which can be perturbed by ectopic activation of ACVR1, a receptor of Bone Morpogenetic Protein (BMP). These initial findings raise further questions. Are oriented cell divisions sufficient to transition from the disordered, mesenchymal condensation to tissues consisting of cell columns? What roles do cell behavior and mechanical interactions play in the formation and maintenance of columns? Is iterative growth in form of added cell layers or additional columns beneficial to the maintenance of the cellular order in the tissue, or does the tissue need to overcome mechanical challenges to enable this iterative growth?

Here, we aim to illuminate key principles governing embryonic cartilage formation and growth by simulating the process using a cell-based computational model. Cell-based computational models have a long history of helping to identify simple rules that contribute to the emergence of order and pattern formation in biological tissues. For example, placement of hair bristles in *Drosophila* can be explained by simple interactions between Notch and Delta signalling [2, 3]. Similarly, mammalian blastocyst formation has been shown to rely on few simple principles, such as differential adhesion and signalling [4]. Cell shapes in growing epithelial tissues can be explained using simplified descriptions of cell mechanical properties and cell-cell interactions [5, 6]. Cell-based computational models have also been widely applied in cancer [7], angiogenesis [8], and other contexts.

Multiple types of cell-based computational model exist, and different modelling paradigms consider cells and their shape at varying levels of detail. For example, cell-center based models consider cells as overlapping spheres [9], whereas vertex models represent epithelial cells as polygons [10]. These models both differ from on-lattice approaches in which space is represented by a lattice. Lattice sites can be occupied by individual cells in so-called Cellular Automaton models [11], or cells can extend across multiple lattice sites in Cellular Potts models [12]. Several mathematical and computational frameworks have been developed which provide modular and adaptable implementations for cell-based computational models. Examples of such frameworks are Chaste [13], CompuCell3D [14], PhysiCell [15] and Morpheus [16].

Here we use a cell-center based model. Chondrocytes have round shapes that lend themselves to the approximation by spheres, which is an inherent component of such models. We implement our model in Chaste, which provides sufficient functionality to enable our studies, such as existing implementations for center-based models, and the modularity to adapt tissue geometry, cell-cycle progression, and cell-cell interactions.

Our approach extends previous efforts on designing mathematical and computational models of cartilage. Kaucka et al. used a cellular automaton model to identify the necessity of oriented cell divisions for the maintenance of columns. Since cellular automaton models operate on a lattice they cannot represent effects from mechanical interactions, and hence this model was not able to answer the further questions outlined above. In another study, Lycke et al. designed an off-lattice computational model of cartilage cells in embryonic femurs of mice, and investigated the distribution of mechanical loads between chondrocytes and ECM [17]. While this study included a careful consideration of cell and tissue mechanics, it did not consider cell division or other cell behaviors. Further models exist to study the formation of mesenchymal condensations in vitro [18, 19]. On the scale of a single cell, models have been designed to describe the molecular pathways that determine cell differentiation events in chondrocytes [20, 21]. On the tissue scale, studies designed continuous mathematical models of embryonic cartilage mechanics that do not account for cell-cell interactions, for example studies on embryonic joint formation [22, 23] or endochondral ossification [24]. Similar continuum models are concerned with the maintenance and mechanics of adult cartilage [25, 26, 27, 28, 29]. Other models study cartilage generation in

engineered tissues [30]. Despite these extensive efforts to accurately model cartilage in embryos and adults, a comprehensive computational investigation of column formation in growth plates remains missing.

Here, our simple, cell-based representation of cartilage formation reveals multiple insights. We confirm that oriented cell divisions are required to establish columnar order in embryonic cartilage. The initial column formation benefits from space between progenitor cells in the lateral direction, and similarly from distance of these progenitor cells to the perichondrial boundaries. Our simulations correctly capture the fact that thicker columns are more disordered, and that this disorder can be reduced if tissue thickness is increased incrementally. We find that oriented cell division and repulsive interactions between cells are not sufficient to enable the intercalation of new cells into the tissue. In this case, our simulations suggest that the generation of space via the deposition of extracellular matrix (ECM) may be a further necessary ingredient.

The remainder of our paper is structured as follows. In the following 'Methods' section, we present our mathematical model and numerical methods. Then, we provide details and results of our computational investigations. Finally, we discuss implications of our results and avenues for future research.

2 Methods

In this section we describe the computational model of cartilage formation from initial aggregates of mesenchymal stem cells. Our model considers the effects of cell division, domain boundaries, and mechanical cell-cell interactions. Specifically, we use a cell-center based model. In cell-center based models, individual cells are represented as spheres [31, 9] that interact through mechanical forces and which are allowed to overlap. Our use of the cell-center based model is motivated by the fact that the main cell type represented in our model, chondrocytes, exhibit a characteristically rounded morphology [32]. In the following, we provide a mathematical description of the dynamics in the model, the force laws that we apply between cells, our chosen initial conditions, and our representation of the cell cycle model. Additionally, we introduce a measure to assess to what extent clonal envelopes form column-like structures. Finally, we provide details of our numerical implementation and describe how to access the simulation source code.

2.1 Cell motion is determined by interaction forces

We denote by $N(t)$ the number of cells that are present at time t. Cells are assumed to experience drag, but not inertia due to the small Reynolds number of cellular environments [33]. The velocity of the midpoint $\mathbf{x}_i$ of cell i is therefore determined by the forces acting on it from its neighbours

$$\eta \frac{\mathrm{d}\mathbf{x}_i}{\mathrm{d}t} = \sum_{j \neq i} \mathbf{F}_{ij}. \tag{1}$$

Here, η denotes the friction coefficient between the cells and the extracellular matrix as the surrounding medium. The sum includes all cells in the system, except cell i. The pairwise force $\mathbf{F}_{ij}$ is applied in the direction between the centers of the cells and its one-dimensional signed magnitude F only depends on the distance between the cells, i.e.

$$\mathbf{F}_{ij} = F(\|\mathbf{r}_{ij}\|) \frac{\mathbf{r}_{ij}}{\|\mathbf{r}_{ij}\|}, \tag{2}$$

where $\mathbf{r}_{ij} = \mathbf{x}_j - \mathbf{x}_i$.

We model the magnitude of pairwise interactions using a repulsion-only, piecewise quadratic force [15],

$$F(r) = \begin{cases} -\mu\left(1 - \frac{r}{s}\right)^2 & \text{if } r \leq s, \\ 0 & \text{otherwise.} \end{cases} \tag{3}$$

Here, $r = \|\mathbf{r}_{ij}\|$ denotes the distance between the cell pair and μ the spring stiffness, i.e. the strength of the repulsive interactions. Furthermore, cells that are further apart than the rest length s do not exert forces on each other. Throughout, s is defined as 1.0 cell diameter and can be thought of as the sum of the radii of two interacting cells. If cells are within one rest-length of each other, they push each other away.

While cell adhesion plays a role in the formation of the initial mesenchymal condensation, cell adhesion molecules are not present once differentiation into cartilage starts. Instead, the proliferating chondrocytes are surrounded by extracellular matrix preventing them from forming adhesive bonds with their neighboring cells [32], motivating our use of a repulsion-only force.

2.2 Cell proliferation

Cell division events alter the system of ODEs (1) by introducing new cells and changing neighborhood arrangements. More specifically, cell proliferation generates the dynamical behavior of the cell population in the following sense. The placement of daughter cells with significant overlap results in localized tensions which propagate through the cell population, pushing cells apart until the whole system reaches a mechanical equilibrium.

For a given cell division direction, two daughter cells of equal radius are placed with a fixed separation distance r_0 between them in a way that the former position of the mother cell lies in the middle. The cell division orientation can be chosen to be oriented or random (uniformly distributed in any direction). Throughout, oriented cell divisions are implemented such that the division direction is along the z-direction (i.e. vertical, see discussion of geometry and initial conditions below.)

To determine the timing of cell division events, we employ a cell cycle model containing two phases. The first cell cycle phase has a fixed duration g_1, while the duration of the second cell cycle phase is exponentially distributed with mean g_2. This choice of cell cycle model prevents synchronicity of cell divisions and ensures that neighboring cells do not divide simultaneously. This helps to maintain the quasistatic limit of our simulations (see Section 2.4). Similarly, including a fixed duration phase prevents immediate successive divisions.

We call the collection of cells arising from a common mesenchymal or perichondrial ancestor a *clonal envelope*. Kaucka *et al.* showed showed that the number of cells in each clonal envelope was related to chondrocyte maturation speed. To reflect the existence of such a control mechanism (without modeling the biochemical details), we limit clonal envelopes by default to contain $n_{\max} = 4$ cells in our model, meaning that cells cease to proliferate once the envelope size reaches this limit.

2.3 Initial and boundary conditions

To study both the primary process of the initial formation of the cartilage sheet and the secondary process of growth through the subsequent insertion of new clonal envelopes into pre-existing cartilage, we use two different initial conditions which we describe in the following.

Configuration (i): Cartilage formation from the mesenchymal condensation

Biologically, the cartilage sheets considered here are formed from an initial condensation of mesenchymal cells [34]. The formation of the mesenchymal condensation itself is a complex, highly regulated process involving cell recruitment, migration, and condensation [35, 34]. Once

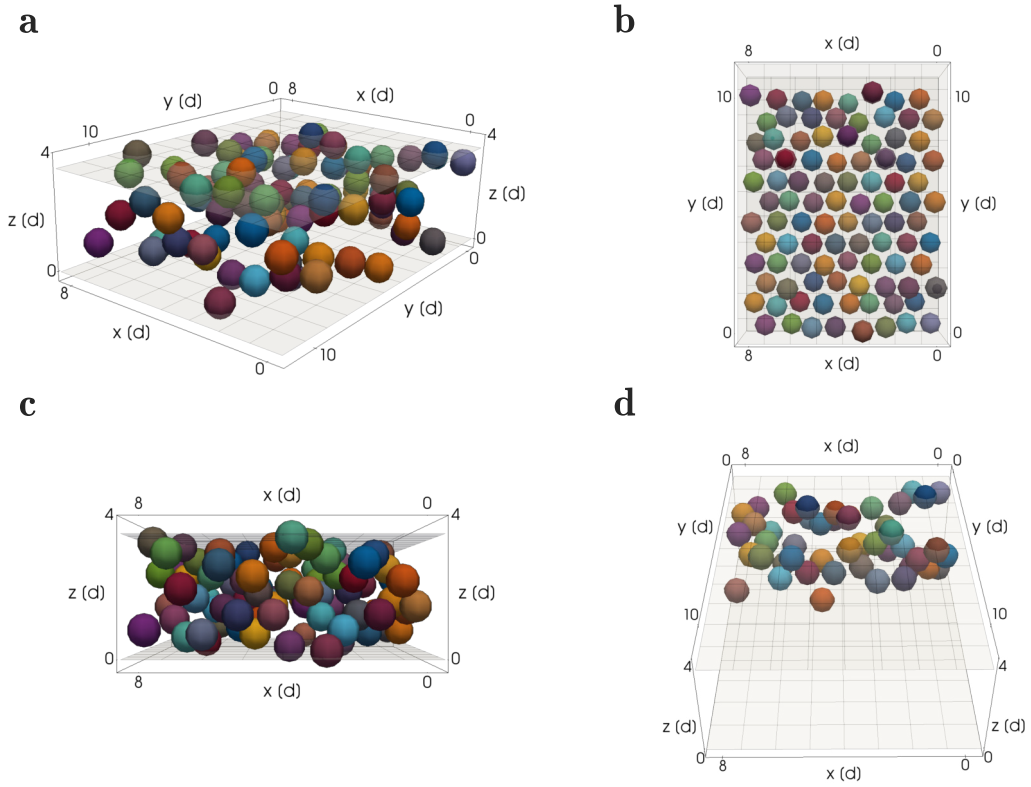

Figure 1: Initial configuration of the mesenchymal condensation used in the simulations. Cells were randomly colored and will pass on their color to their progenity. Cells located in close proximity have different colors so that different growing clonal envelopes will be easily distinguishable at later time points in the simulation. (a) General 3D view visualizing the overall shape of the mesenchymal condensation as well as the lower and upper boundary planes situated at their default values of $l = 0$ and $u = 3.5\,d$. (b) View from above of the cell arrangement in the lateral x-y plane according to a perturbed honeycomb mesh. (c) Sideways view to visualize the spread of the mesenchymal cells in the transversal z direction, filling the space between the upper and lower rigid boundary planes. (d) Application of the threshold to the number of clonal ancestors that is used to visualize example clonal configurations throughout the results section.

progenitor cells are in place, they differentiate into chondrocytes which mature and cease to proliferate. The initial conditions of our simulations are designed to reflect these mesenchymal condensations at the stage where progenitor cells have condensed, just at the beginning of chondrocyte differentiation.

The spatial configuration of the mesenchymal condensation reflects the geometry of the mature sheet (Figure 1). We place 72 cells to generate a condensation 8 cells wide in the x-direction and 12 cells long in the y-direction, while being comprised of a single cell in the z direction. The exact dimensions of the mesenchymal condensation have been chosen large enough to collect robust statistics on the 'order' of each column, while at the same time being low enough to ensure simulation times of a single run do not exceed a few minutes so that parameter sweeps can be executed in a reasonable amount of time. In the direction of lateral expansion, i.e. within the x-y plane, the cells are arranged on a honeycomb lattice (Figure 1 (b)), in which distances between neighboring cells are set to $1.075\,s$. Here, s denotes the rest length, chosen by default as one cell diameter. This arrangement leads to cells being densely

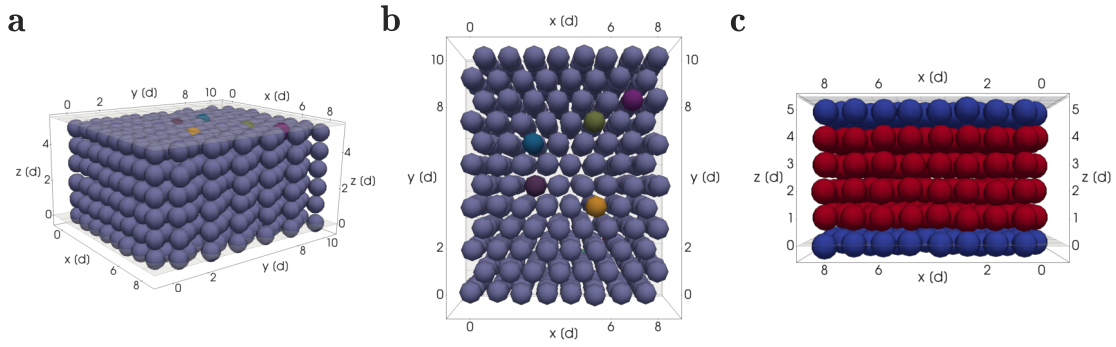

Figure 2: Initial configuration (ii) for the study of inserting new columns into an existing cartilage sheet. (a) Three dimensional view. (b) View from above of the cell arrangement in the lateral x-y plane according to a perturbed honeycomb mesh. The differently colored perichondrial cells in the top layer seen in (a) and (b) divide giving rise to clonal envelopes. (c) Sideways view to visualize the layers of chondrocytes (in red) and perichondrial cells (in blue) between the upper and lower rigid boundary planes.

packed in the direction of lateral expansion, mirroring the biological requirement of a high cell density to initiate the differentiation into chondrocytes [DeLise et al., 2000]. In the transversal direction z, we let individual cells be spread out between the upper and lower rigid boundary planes located at $z = l$ and $z = u$, as shown in Figure 1 (c). Specifically, z-locations are chosen uniformly at random in $z \in (l, u)$. These boundary planes model the mechanical influence of the surrounding perichondrial tissue. Note that we do not impose any boundary conditions in the x-y plane.

Additionally, a perturbation drawn uniformly from $[0, p_{\max}]$ is added to each coordinate of all cell midpoints to allow for biologically realistic variations on the cell positions. Note that the rigid boundaries of the condensation are enforced at the cell midpoints, meaning that parts of the cell's spheres can surpass the boundary planes as visible in Figure 1. The value of $p_{\max} = 0.1\, d$ is chosen small enough as to not significantly alter the geometrical arrangement of the mesenchymal condensation.

For visualization purposes, we consider a view looking along the y axis onto the middle of the condensation, by applying a threshold to the number of clonal ancestors (Figure 1 (d)). This enables us to observe the geometrical shape of clonal envelopes in the middle of the sheet. We use this view when visualizing example snapshot configurations of the mesenchymal condensation and the forming cartilage at different time points.

Configuration (ii): Cartilage growth through insertion of new clonal envelopes into a pre-existing sheet

In [1], the authors could identify a clonal relationship between chondrocyte columns and individual perichondrial cells, suggesting that during cartilage expansion new clonal envelopes were seeded from the latter cells located at the periphery of the pre-existing cartilage. Building on this hypothesis, we designed a second simulation setup to study the insertion of new columns as follows. We modeled a pre-existing sheet through layers of cells (Figure 2 (a)). These were arranged as transversal columns according to an underlying hexagonal lattice in the x-y direction (Figure 2 (b)). The number of cells in the x and y dimension were the same as for the mesenchymal condensation. We used four layers of chondrocytes and added two layers of perichondrial cells, one above and one below the chondrocyte sheet, still within the rigid boundary planes (Figure 2 (c)). Perichondrial cells differed from chondrocytes in their cell division dynamics and orientation, dividing parallel to the sheet asymmetrically into one perichondrial daughter

Parameter	Description	Value
T	Simulation end time	$80\,a.u.$
Δt	Simulation time step size	$0.0083333\,a.u.$
η	Friction coefficient	1.0
n_x	Number of cells in x-direction	8
n_y	Number of cells in y-direction	12
n_z	Number of cells in z-direction	1
$p_{\max}$	Maximum perturbation of initial coordinates	$0.1\,d$
u	z-coordinate of upper boundary plane	$3.5\,d$
l	z-coordinate of lower boundary plane	$0\,d$
$n_{\max}$	Maximum number of cells per clonal envelope	4
s	Rest length	$1.0\,d$
μ	(Repulsive) spring stiffness	20.0
g_1	G1-phase duration (fixed)	$3\,a.u.$
g_2	Mean G2-phase duration (exponentially distributed)	$10\,a.u.$
r_0	Initial separation distance between daughter cells	$0.3\,d$
c	Scaling of distances between neighboring midpoints in the lateral x-y-plane	1.075

Table 1: Model and numerical parameters along with their default values. These are used across all experiments unless specified differently for individual experiments. Length scales are measured in cell diameters d. Time scales are measured in arbitrary time units $a.u.$.

cell and one chondrocyte daughter cell. A fraction of the perichondrial cells in both layers were "activated", i.e. chosen to divide once in order to insert new columns into the pre-exisiting sheet (colored in Figure 2 (a)). Their progenity cells inherited the coloring to enable identification of clonal envelopes. Perturbation of the initial coordinates, inital spacing between cells in the x-y-plane and the properties of the rigid boundary planes above and below the sheet were chosen consistent with initial configuration (i). We denote this initial configuration as configuration (ii).

2.4 Model parameter values and quasistatic limit

Cell cycle duration of proliferating chondrocytes in the clonal patches is on the order of 24 hours as estimated from Figure 4 in [1]. We expect mechanical relaxation to occur on a time scale of minutes, i.e. roughly three orders of magnitude faster than cell division. This large difference in time scales allows us to assume that our model operates within a quasistatic limit, in which the cell population regains a mechanically stable configuration in between subsequent cell division events. We choose a repulsive force strength of $\mu = 20.0$ and a friction strength of $\eta = 1.0$. The ratio between these two parameters η and μ determines the mechanical relaxation time scale in the simulations, since both parameters only occur as multiplicative constants in Equations (1) and (3).

To reflect the fact that our time scales are only loosely coupled to the real physical units, we measure time in *arbitrary time units* which we abbreviate as $a.u.$. Simulation end time is chosen as $80\,a.u.$, which is sufficiently long for final cell population configurations to reach a mechanical equilibrium. Mean cell cycle duration is chosen as $13\,a.u.$ to ensure that simulation wall time remains sufficiently short while conserving the quasistatic equilibrium. Here, the duration is split between the phases as $g_1 = 3\,a.u.$ and $g_2 = 10\,a.u.$.

All parameter values used in the simulation of our model are summarized in Table 1, along with their default values.

2.5 Randomness in the model

Randomness enters the model in four ways, firstly through the perturbation of the initial cell coordinates, secondly through the distribution of the G2 cell cycle phase (and as a result the distribution of cell division times), thirdly, if cell division is not set to take place in an oriented fashion, through random cell division directions, and lastly, through the choice of activated perichondrial cells in initial configuration (ii). We therefore run numerical experiments for each parameter setting with 8 different random seeds and average over the results.

2.6 Metric for evaluating order in the cartilage sheet

To evaluate the quality of the clonal column growth we measured the shape of each clonal envelope. For each envelope we calculated its projection area by multiplying the maximum deviation in both x and y direction. We then averaged over all envelopes to obtain the average envelope projection area a as

$$a = \frac{1}{\#\text{envelopes}} \sum_{\mathcal{E}\text{: clonal envelope}} |\max_{\text{cells}\in\mathcal{E}} x - \min_{\text{cells}\in\mathcal{E}} x| * |\max_{\text{cells}\in\mathcal{E}} y - \min_{\text{cells}\in\mathcal{E}} y|.$$

The smaller a is, the more column-like the geometrical shape of the average clonal envelope is.

2.7 Simulation procedure

Simulation of our cartilage growth model proceeds as follows. The cell population is created according to the initial configuration and cells are initialized at a given position in space. Time is then advanced in discrete time steps until the end time is reached. At each time point, both cell states and positions are updated in a two step process. First, all cells advance through the cell cycle by the elapsed time. If a cell is ready to divide, a new daughter cell is created and inserted into the population. The duration of each cell's G2 phase is drawn individually from an exponential distribution at cell initialization.

Once all possible cell division events have been carried out, the positions of all cells in the population are updated. Equation (1) is solved numerically using the forward Euler method [36]. Cell midpoint coordinates are updated by adding the sum of the current force interactions scaled with the current time step length Δt as

$$\mathbf{x}_i^{\texttt{new}} = \mathbf{x}_i^{\texttt{old}} + \Delta t \sum_j \mathbf{F}_{ij}^{\texttt{old}}. \tag{4}$$

We use the timestep $\Delta t = 0.0083333\, a.u.$, the default value in the Chaste software [13]. Once cell positions are updated, simulation time is advanced and the next time step begins. This loop continues until the simulation end time is reached.

2.8 Code availability

Our model is implemented using the open-source simulation software Chaste (Cancer, Heart and Soft Tissue Environment) [13], specifically its cell-based component. All model specific code including scripts for data analysis and figure generation is available on GitHub at `https://github.com/somathias/CartilageCBM/`.

3 Results

The earliest mesenchymal condensations giving rise to the basic shape of the developing mouse cranium can be observed from day E12.5 [1]. Already at day E13.5 the presence of transversely oriented doublets is observed, with the characteristic arrangement of transversal clonal

columns in the resulting sheet-like cartilaginous elements being present at E17.5. During this time, the finer features of the nasal part of the cranium are added through subsequent waves of new mesenchymal condensations added to already existing cartilage which in turn again develop to exhibit the highly ordered microgeometry of clonal columns. How the columns are initially formed from each condensation differentiating into chondrocytes and which mechanical mechanisms contribute to the generation of these structures remains unclear due to the lack of possibility to observe the process in-vivo through live-imaging. A computational model can fill this gap and propose possible mechanisms. In this section we investigate how the distinct geometrical shape of clonal columns can form from initially condensed mesenchymal ancestor cells, before moving on to how column intercalation into pre-existing cartilage may be achieved.

A repulsion-only force and oriented cell division enable column formation.

When sheet-like cartilaginous elements are formed from an initial mesenchymal condensation e.g. in the nasal capsule of the embryonic mouse, clonal envelopes arrange themselves very robustly into highly ordered columnar shapes. Since progenitor cells arising from different ancestors are likely to be obstructed by neighbours in the lateral x-y direction, but not in the transversal z direction, we asked whether a regular spacing of initial mesenchymal ancestor cells combined with randomly oriented divisions may be sufficient to induce the growth of clonal columns. We arranged cells according to the initial configuration (i) described in Figure 3 (a), c.f. Section 2.3. We then simulated cartilage formation as described in Section 2.7. We let cells divide in randomly chosen directions until each clonal envelope contained 4 cells. Rigid boundary planes above and below the condensation constrained cell positions to the developing sheet, as a substitute for the mechanical influence of the surrounding tissue.

We found that this simulation was unsuccessful in generating ordered columns. Clonal aggregates observed for this case in Figure 3 (b) do not show a recognizable geometrical order, and clonal envelopes are overlapping. In [1], experimental evidence for the orientation of cell divisions into the developing sheet was given. Similarly, their use of mathematical modelling suggested that the presence of a two-sided gradient directing the division direction was necessary for the columnar growth of the clonal envelopes. Moreover, by experimentally increasing signalling of bone morphogenetic proteins (BMP), the authors were able to disrupt the correct formation of columns, leading to the conclusion that either BMP ligands are responsible for the gradient itself, or their increased expression overshadows any gradient established by other molecules. As the exact molecular mechanism of the gradient formation remains unknown, we deterministically set the division direction in our computational model to align with the z-axis. As a result oriented cell division happens transversely to the main expansion direction of the sheet. As predicted, inclusion of this mechanism led to clonal envelopes forming column-like structures (Figure 3 (c)).

The visually observed differences in panels (a) and (b) can be quantified using the envelope projection area metric introduced in Section 2.6 for measuring the order of cartilage columns. The metric multiplies the maximum spread in x and y direction among the coordinates of the cells belonging to each clonal envelope and then averages over all envelopes. If envelopes on average have a column-like shape, the metric is small, and conversely, unordered shapes result in large values. Figure 3 (d) depicts the envelope projection area as a function of time for both the case with randomly chosen cell division directions and the case when cells divided in an oriented fashion. The envelope projection area increased rapidly for the random cell division case, whereas it stayed small for the oriented division case. It is hence clear that independent of the particular random seed, clonal patches consistently grew in column-like structures when allowed to divide upwards, in contrast to them exhibiting no geometrical order when division directions were chosen randomly. We conclude that oriented cell division in combination with an repulsion-only force (no adhesive forces necessary) is sufficient for column formation from a mesenchymal condensation.

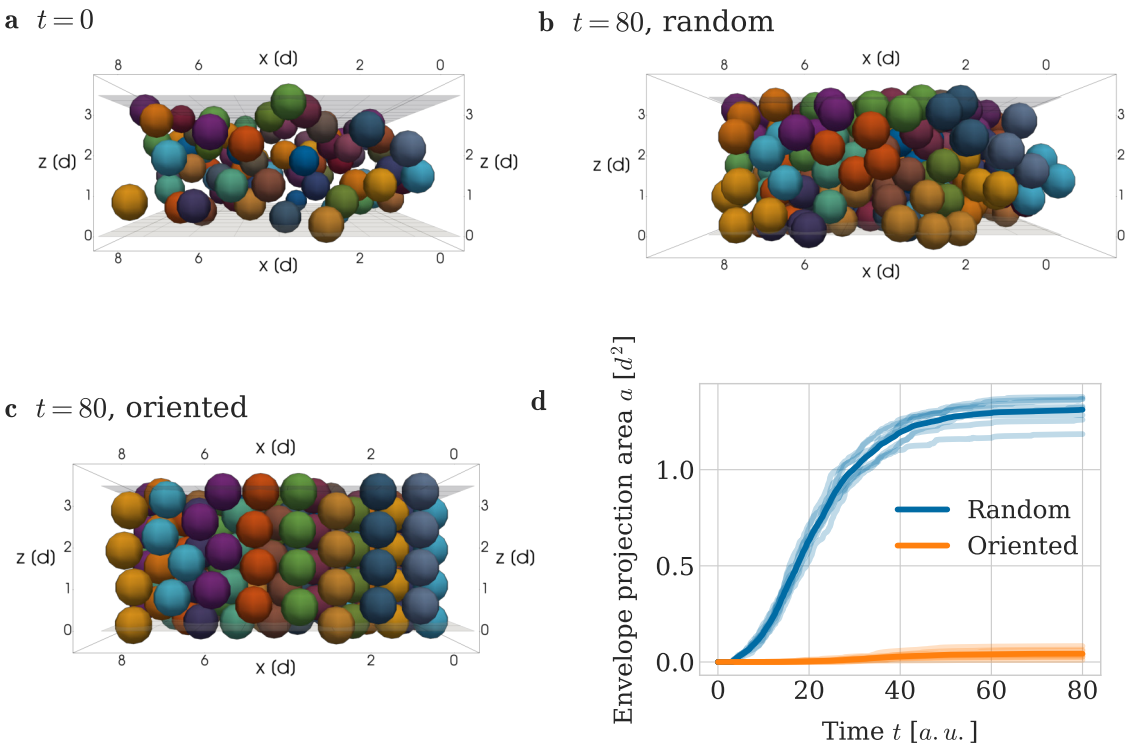

Figure 3: Impact of oriented and random cell division directions on column formation. (a) Initial configuration of mesenchymal condensation (view cuts through the middle), used for both experiments with oriented and random cell division directions. (b, c) Example configurations at $t = 80\,a.u.$ when using (b) random and (c) oriented cell division directions and the same fixed random seed. Same view as in (a). Colors are consistent across plots (a), (b) and (c) with cells within a clonal patch inheriting their color from their ancestor. Ancestor cells located in close proximity were assigned different colors so that clonal envelopes were easily distinguishable. (d) Envelope projection area over time for oriented and random cell division directions. The thick line denotes the average over 8 different random seeds, the individual data of which are plotted with increased opacity.

Column growth benefits from more extracellular matrix between cells

Having identified a mechanism for the growth of column-like structures from the mesenchymal condensation, we next asked how robust this mechanism is to changes in the amount of extracellular matrix between cells dictating the spacing between cells in the initial spatial configuration of the population. To this end, we considered the scaling of the cell arrangement in the lateral x-y plane as depicted in Figure 4 (a). Biologically, increasing the distance between the individual ancestor cells with a scaling parameter $c > 1.0$ can be interpreted as there being more extracellular matrix between the mesenchymal ancestor cells. Again, we let cells divide in an oriented fashion until clonal envelopes contained four member cells, while leaving all others simulation aspects unchanged to the previous simulation. For a scaling parameter value of $c = 1.0$, corresponding to a minimal amount of extracellular matrix, clonal envelopes exhibited column-like structures, yet the order of the column was decreased and columns were less straight (compare Figure 4 (b) to Figure 3 (c)). Increasing the scaling parameter to values above our default value of $c = 1.075$, e.g. to a value of $c = 1.1$, increased the smoothness and straightness of the columns formed by the clonal aggregates (Figure 4 (c)). Again, this visual finding was quantified by the envelope projection area metric a (Figure 4 (d)). Taken together, these experiments demonstrate that the robustness of ordered column formation increases with

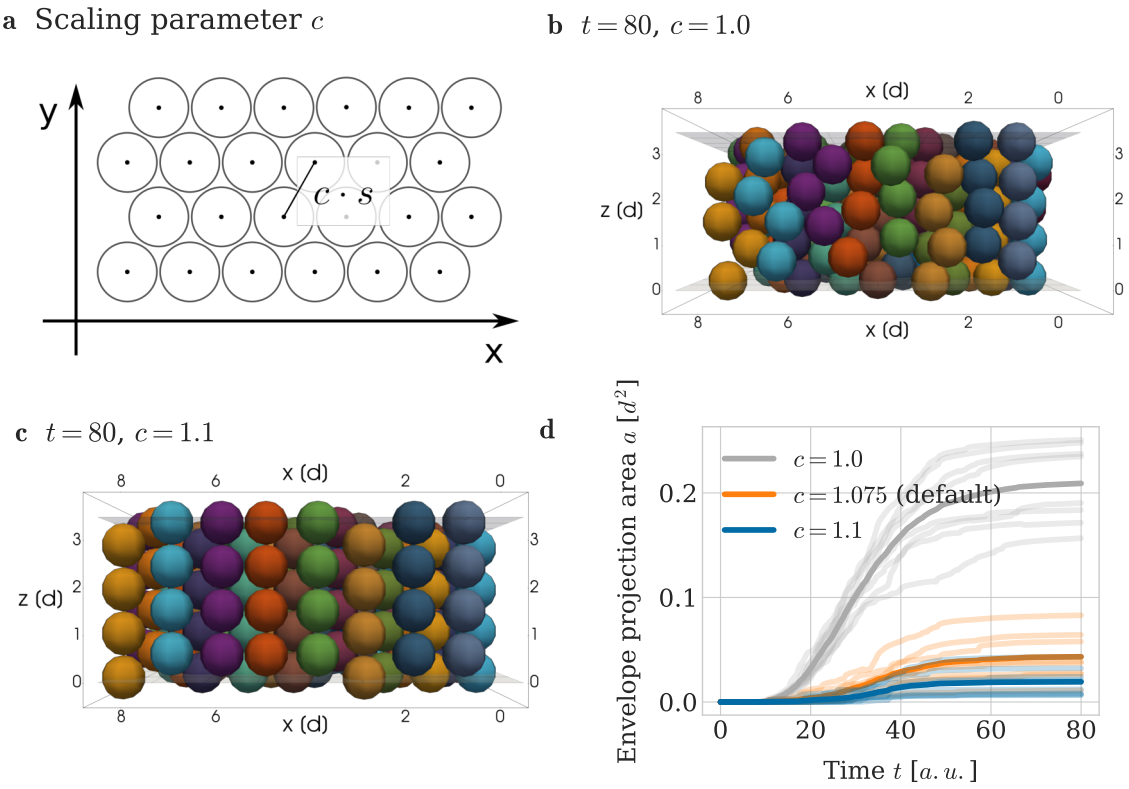

Figure 4: Impact of scaling of the initial configuration of the condensation in the x-y-plane on column growth. (a) Visualization of scaling parameter c. Note that the condensation used in the simulation has 8 cells in x- and 12 cells in y-direction. (b,c) Example simulation snapshots at $T = 80\,a.u.$, cut through the middle of the mesenchymal condensation for a scaling of (b) $c = 1.0$ and (c) $c = 1.1$. (d) Patch projection area over time for different scaling values c. Opaque lines denote the results from different random seeds and the thick line denotes the average over all random seeds.

larger initial spacing between cells which intuitively leads to less mechanical tension in the lateral direction as the columns grow.

Column growth benefits from distance to the perichondrial boundary.

The developing sheet-like cartilages in the chondrocranium are surrounded by a layer of perichondrial cells [1]. This layer is only a few cells wide and formed from mesenchymal ancestors located at the boundary of the mesenchymal condensation. For the process of endochondral ossification in the context of long bone development, it is well understood that the perichondrium plays an important role through several functions such as providing signalling cues controlling proliferation and differentiation of the chondrocytes within the condensation [37, 38], giving rise to cells that establish the bone collar as well as promoting the formation of blood vessels in the bone [39]. The perichondrium is structurally different to the cartilage as the perichondrial cells exhibit a flat morphology and are situated in a matrix characterized by a horizontal arrangement of collagen fibers [40]. We here model the mechanical influence of the surrounding tissue—including the perichondrial cell layers—on the developing cartilage through the use of rigid boundary planes. Next, we asked how the distance of the mesenchymal condensation to these perichondrial boundary planes affected the geometrical order of the formed clonal envelopes. Having cells located away from the boundary can be interpreted as there being an increased amount of soft hyaline matrix.

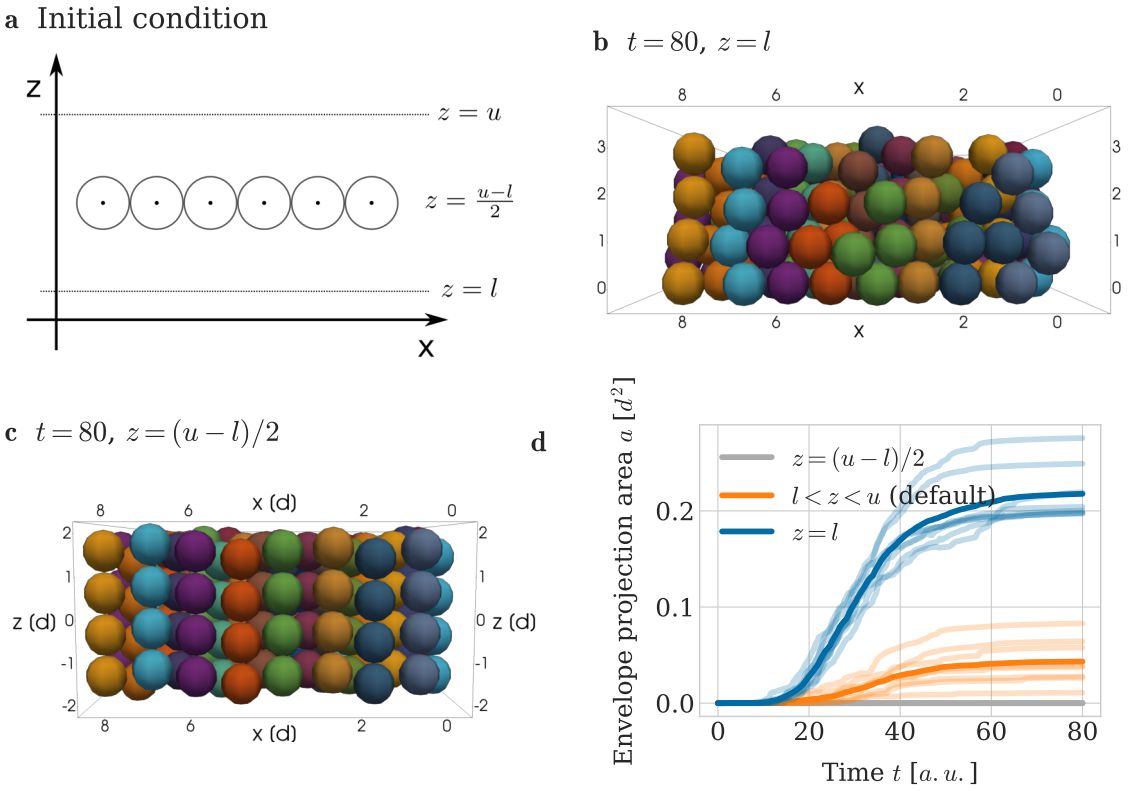

Figure 5: Impact of distance to perichondrial boundary on column growth. (a) Visualization of initial configuration. (b,c) Example simulation snapshots at $T = 80\,a.u.$ for all cells of the mesenchymal condensation being placed at (b) the lower perichondrial boundary ($z = l$) and (c) the middle between upper and lower boundary ($z = (u - l)/2$). (d) Patch projection area over time for the different initial configurations. Opaque lines denote the results from different random seeds and the thick line denotes the average over all random seeds.

Instead of spreading out the cells of the mesenchymal condensation between the upper and the lower boundary planes, we let all mesenchymal ancestor cells be situated in a single layer at two different heights (Figure 5 (a)). In a first simulation, we placed cells at the lower perichondrial boundary $z = l$ and then let them divide in an oriented fashion. This resulted in clonal envelopes with visibly less ordered geometrical shapes (Figure 5 (b)). In a second simulation, we instead arranged all mesenchymal cells in a flat sheet situated at the middle between the boundary planes, i.e. at maximum distance from both boundaries, $z = (u - l)/2$ and obtained perfectly straight column growth. We conclude ECM and mesenchymal space between initiating column formation benefits column straightness.

Trade-off between column thickness and order

Cartilage sheets are found in different parts of the developing skull such as in the nasal capsule, basisphenoid and the inner ear. Depending on their location their thickness differs with basisphenoid and inner ear cartilage being on average thicker than olfactory cartilage (see [1], Figure 8, panels B, D, F and H, results for the littermate wild type control). This motivated us to study how the geometrical order of the clonal shapes depended on the thickness of the sheet. Since the thickness of the sheet is controlled by the number of clones per envelope, we varied the maximum number of cells $n_{\max}$ allowed in each envelope and adjusted the height u of the upper boundary plane accordingly to ensure space for perfectly ordered columns (Figure 6 (a)). Starting from our default mesenchymal configuration in which z-coordinates are drawn uniformly

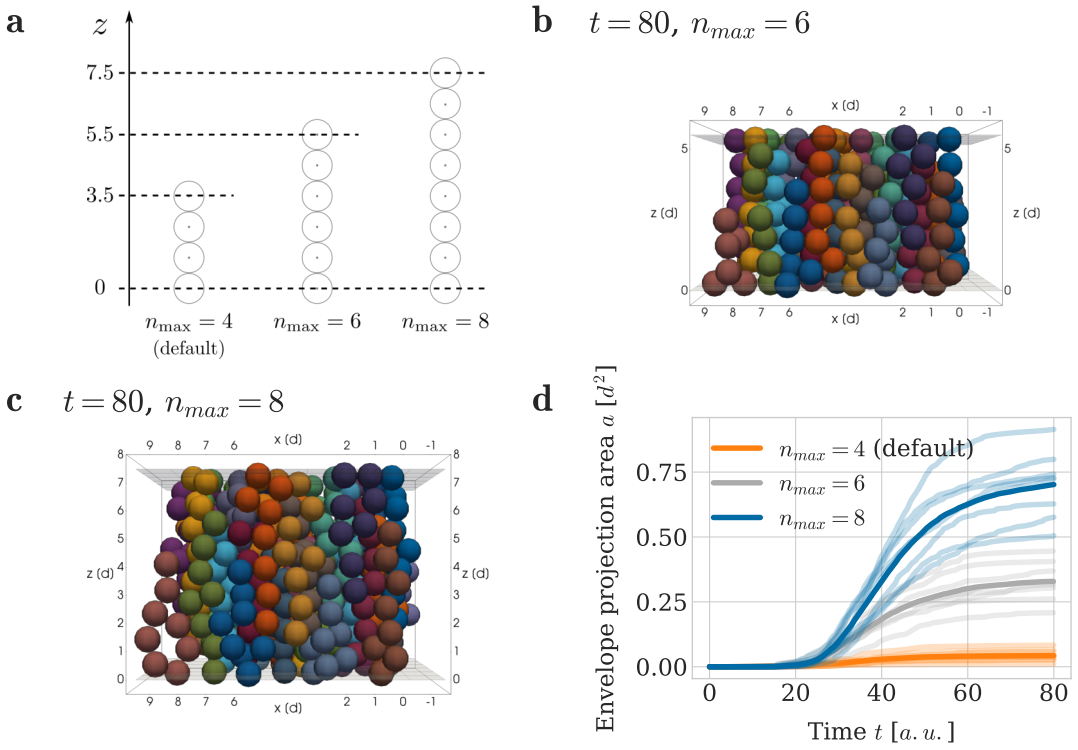

Figure 6: Impact of column thickness on column order. (a) Location of upper rigid boundary plane u for different clonal envelope sizes $n_{\max}$. (b, c) Example simulation snapshots at $T = 80\,a.u.$ for clonal envelope sizes being limited to (b) $n_{\max} = 6$ cells and (c) $n_{\max} = 8$ cells. (d) Patch projection area over time for different clonal envelope sizes. Opaque lines denote the results from different random seeds and the thick line denotes the average over all random seeds.

from the distance between the (adjusted) boundary planes, chondrocytes stopped dividing once the size of their clonal envelop reached $n_{\max}$. Visual inspection of example simulations for $n_{\max} = 6$ (Figure 6 (b)) and $n_{\max} = 8$ (Figure 6 (c)) showed that for thicker sheets the geometrical order of the clonal shape decreased. Columns were more likely to be two cells wide when consisting of 8 cells (Figure 6 (c)), although we stress that clonal envelopes continued to show a clear orientation transversal to the main lateral direction of expansion. Again, quantifying the results through the use of the patch projection area, confirms that column order decreases with sheet thickness (Figure 6 (d)). Additionally, it confirms that clonal envelopes comprised of 8 cells which divided in an oriented fashion are more ordered than envelopes with 4 cells and random cell division directions. These experiments suggest a trade-off between cartilage thickness and order in the cellular micro-structure of the cartilage.

It is more efficient to keep order by increasing column size, than to grow larger columns from scratch.

To accommodate the significant growth during development, cranial cartilage sheets in the mouse embryo need to be scaled accurately both in longitude and in thickness. As discussed in the previous subsection, growing thicker sheets through continuous proliferative phases results in a decrease in geometrical order with increasing number of clones per envelope. Next, we were interested whether a mechanism of sequential proliferative phases, where the number of clones is initially restricted and later increased, could benefit column growth. To this end, we ran a simulation based on a step wise profile for the limit of cells per envelope $n_{\max}$ (Figure

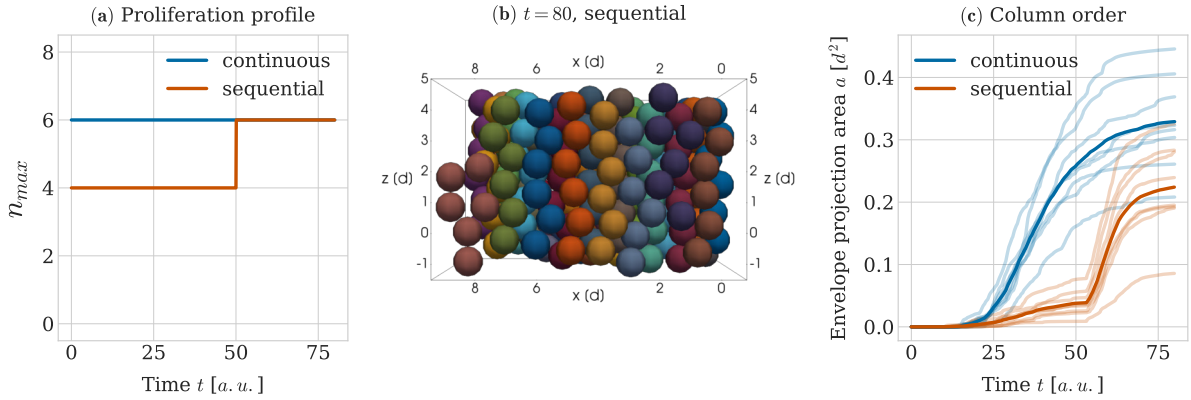

Figure 7: Impact of sequential proliferative phases on column growth. (a) Profile of the limit on the number of cells per clonal envelope $n_{\max}$ over time with either a single continuous proliferative phase (blue line) or two sequential proliferative phases with a step wise increase in the limit (red line). In either case the goal is to grow clonal columns 6 cells high. (b) Example simulation snapshot at $T = 80\,a.u.$ for the sequential proliferative profile. (c) Envelope projection area over time for the two different proliferative profiles (continuous and sequential). Opaque lines denote the results from different random seeds and the thick line denotes the average over all random seeds.

7 (a), red line). Initially, the limit was chosen as 4 cells per envelope and then increased to 6 cells at $t = 50\,a.u.$. This time point was chosen such that all clonal envelopes had time to grow to the limit of 4 cells and to mechanically relax as well. As comparison, we used simulations in which the limit $n_{\max}$ was chosen as 6 cells from the beginning (Figure 7 (a), blue line). Comparing example snapshots for the different proliferative profiles, we observed that if growth happened in sequential proliferative phases, envelopes had a higher chance of spanning the entire height between the lower and upper rigid boundaries (Figure 7 (b)). In contrast, if clones were continuously proliferating up to the final $n_{\max}$ value, shapes often resulted in shorter columns two cells wide (Figure 6 (b)). These qualitative differences were confirmed quantitatively with a smaller average envelope projection area (Figure 7 (c)). Hence, our simulations indicate that iterative growth of columns observed in Kaucka *et al.* is beneficial for the maintenance of column order.

In addition to finer features of the developing mouse cranium being added by the induction of new mesenchymal condensations, the existing cartilage grows in size as well, while accurately keeping shape and proportions. In [1], the authors show that the complex structure of transversal columns in sheet-like cartilage allows for this to be done accurately by introducing new columns into the already existing sheet. We now apply our understanding about how columns form initially to study the principles of this secondary scaling process.

Oriented cell division is not sufficient for column insertion.

We initially assumed that the principles sufficient for initial column formation should also enable scaling of the sheet through column intercalation. To test this hypothesis, we simulated the insertion of new columns based on configuration (ii) (see Section 2.3), where columns of chondrocytes were arranged into a cartilage sheet with a perichondrial layer situated both above and below. Activated cells in the perichondrial layers divided once parallel to the main expansion direction of the sheet, thereby seeding a new clonal envelope. Subsequent divisions of the chondrocyte clones were then again oriented transversally into the sheet, as was the case when forming columns initially from the mesenchymal condensation. We set the maximum number of cells per clonal envelope to $n_{\max} = 5$ to allow columns to potentially span the width

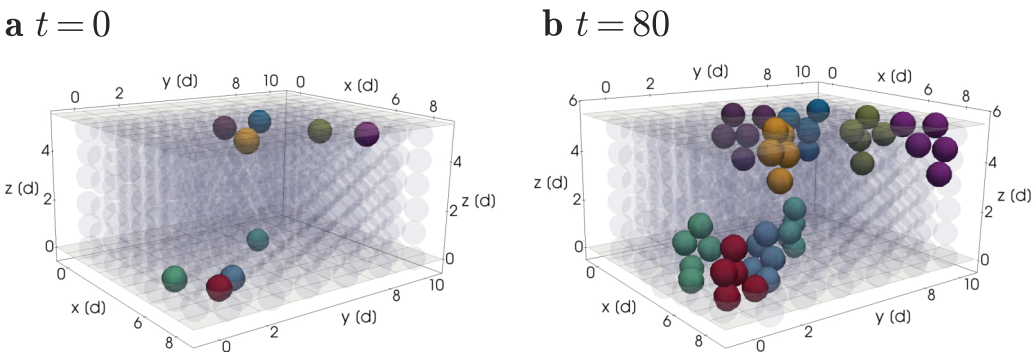

Figure 8: Intercalation of clonal envelopes into pre-existing cartilage sheets. An example simulation result is shown at (a) $t = 0$ and (b) $t = 80\,a.u.$. The pre-existing cartilage is not shown for better visibility of the shape of new clonal units.

of the sheet. The original perichondrial cell was not counted towards this limit (even so it is depicted in the same color as clonal envelope it seeded).

With this setup, clonal envelopes were able to insert themselves into the pre-existing sheet, but not in the shape of clearly visible columns (Figure 8). Instead they consistently formed aggregates that were two cells wide and only reached to the middle of the sheet. Using the same patch projection area metric as before, we could confirm that the geometrical order of the clonal envelope shape was decreased compared to a five cell column grown directly from the initial mesenchymal condensation (Figure 10 (a)). This lead us to conclude that orientated clonal cell division is not sufficient to insert well-formed columns that span the whole sheet width.

New columns can grow into existing cartilage if there is space.

Our previous results indicated that column formation benefits from increased amounts of extracellular matrix, manifesting as gaps in the spatial arrangement of the mesenchymal ancestor cells in configuration (i). We hypothesized that the same principle holds true for the insertion of new clonal envelopes into pre-existing cartilage. To test this hypothesis, we considered a portion of the cartilage sheet described in configuration (ii), measuring 5 columns wide and 5 columns deep and deleted the middle column (Figure 9 (a)). We then chose a perichondrial cell next to the missing column to divide into the available space. Its chondrocyte progenity was then able to grow into a clearly columnar shape within the cartilage sheet (Figure 9 (b)). We used the projection area metric on the inserted clonal envelope across different random seeds to confirm that, if there was space in the pre-existing cartilage, the average geometrical order of the clonal envelope was similar to a column grown directly from the initial mesenchymal condensation (Figure 10 (b)). To conclude, these results further implicate the importance of the extracellular matrix for the growth of embryonic sheet-like cartilage through the intercalation of clonal envelopes arranged in a columnar shape.

4 Discussion

How cells interact to coordinate morphogenesis is a key question in developmental biology. Here, we investigated this question at the example of embryonic cartilage in growth plates of the skull. Motivated by previous findings in mouse embryos, we wondered how cells arrange into columns from initially disordered mesenchymal condensations.

Using a cell-center based computational model, we confirmed that oriented cell divisions are necessary for column formation. We found that column formation benefits from space between

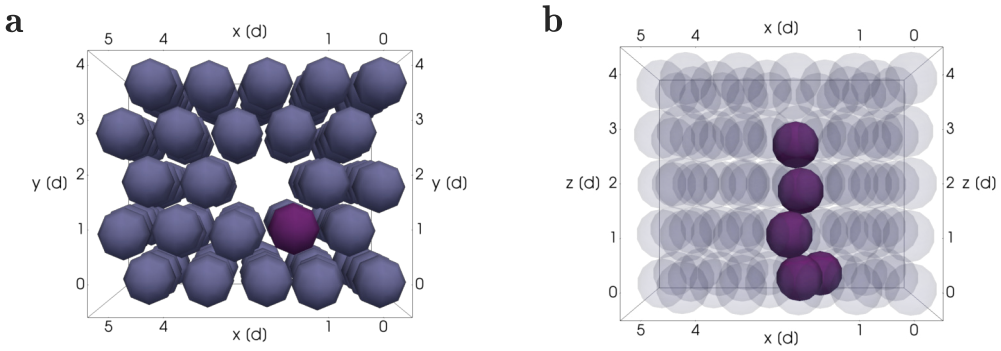

Figure 9: Intercalation of clonal envelopes into pre-existing cartilage sheets with space made available beforehand. An example simulation result is shown at (a) $t = 0$ from below and (b) at $t = 80\,a.u.$ from the side. The purple perichondrial cell in (a) divided into the space provided and seeded the clonal envelope seen in (b).

progenitor cells in the mesenchymal condensation. Our model indicates that tradeoffs between column length and order can be mitigated by iterative growth. We identified that oriented cell divisions are insufficient to ensure that new columns can be inserted into existing tissues, and suggested that extracellular matrix may generate space before new columns are grown.

Our cartilage growth model complements the original mathematical model presented in [1] by a more fine-tuned model of the cellular mechanics. Using an off-lattice approach eliminates possible grid artifacts and offers more flexibility. Importantly, unlike the Cellular Automaton model used in [1] the model developed here explicitly lets cells push on each other as point masses during mechanical relaxation, without relying on ad-hoc rules that are hard to parameterize and to relate directly to biological function. The present model is also able to implicitly represent the presence of extracellular matrix by continuously varying the space between cells. This enabled us to go beyond the previous modeling and investigate how the extracellular matrix can contribute to robustness of ordered column formation as well as study the principles for column intercalation.

The main modeling assumptions made by the cell-center based model concern the representation of cell shape, the assumption that cell interactions occur pairwise and the choice of pairwise interaction force. For our application of cartilage growth and formation, modeling cells as spheres is motivated by the rounded morphology of chondrocytes. Similarly, as the chondrocytes are embedded in extracellular matrix, no cell-cell adhesion takes place between them, which supports both our choice of a repulsion-only force and the validity of pairwise mechanical interactions. Last but not least, there exist several other force functions in the literature used in combination with cell-center based models, exhibiting qualitatively similar force shapes, e.g. the cubic force [41], the generalized linear spring force [13]. However, as all these force functions can easily be parametrized in a way that their biological behavior at the population level agrees well in repulsion-dominated settings [42], we do not expect the exact mathematical formulation chosen to qualitatively affect our results.

Both the modeling done in [1] and the computational model presented in this study confirm that orientated cell division dynamics play an important role for enabling column growth. From the biological data in [1], it is however not distinguishable, whether the division itself is really oriented, or if the initial cell division direction is random and then daughter cells slide around each other until the doublet is oriented transversely to the sheet. In our model, for simplicity we deterministically set the division direction itself parallel to the z-axis and hence perpendicular to the main expansion direction of the sheet. Since we do not observe un-oriented doublets in [1], we can deduce that any sliding of daughter cells would need to take place quickly, resulting

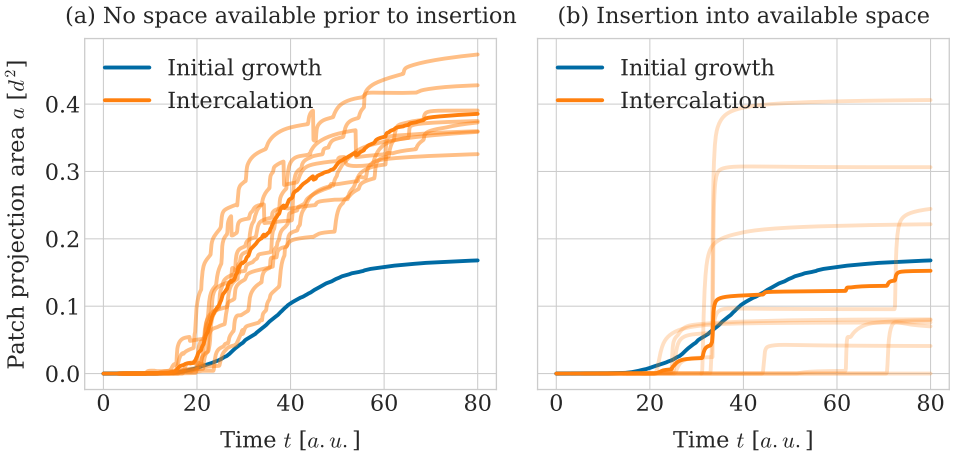

Figure 10: Envelope projection area over time for the intercalation of clonal envelopes into a pre-existing sheet with (a) no available space and (b) with space made beforehand. Opaque orange lines denote the results from different random seeds and the thick orange line denotes the average over all random seeds. For comparison the average projection area for clonal columns comprised of 5 cells grown directly from the initial mesenchymal condensation is shown in both panels in blue (denoted by 'initial growth').

in us being confident that this is a reasonable simplification. Moreover, in contrast to the model used in [1] we do not consider any noise in the cell division if oriented. Instead we perturb the initial arrangement of the progenitor cells in space slightly. The mechanical influence of slightly misaligned neighbors affect dividing daughter cells leading in practice to a perturbation in the orientation of the doublet.

Our results on column insertion indicate that the deposition of ECM is a major component of cartilage morphogenesis. Specifically, additional space between cells that can be generated through the deposition of ECM may facilitate the maintenance of columns, as well the insertion of new columns into existing tissues during growth. This is consistent with the fact that chondrocytes are known secrete large amounts of ECM.

Our model does not explicitly represent the extracellular matrix. Instead our model implicitly captures its effect through two mechanisms. Firstly, space between the cells in our configurations is directly related to the amount of matrix between them. Secondly, the mechanical interactions of the cells with their environment, i.e. the extracellular matrix are governed by the drag coefficient η in Equation (1). It is therefore straightforward to extend our model to study anisotropy in the properties of the extracellular matrix by varying *eta* both in space or in time. As an example, the cartilage itself and the perichondrium surrounding it exhibit differences in the composition of their extracellular matrix and hence differ in their mechanical properties. The matrix surrounding the chondrocytes within the cartilage has a high amount of proteoglycan aggregates and collagen type II making it more soft, whereas the matrix around perichondrial cells is comprised of horizontally aligned collagen fibers of type I [43, 40]. An extension of our current model could then take the different mechanical properties of these two tissues into account by assigning different drag coefficients to these tissues (with eta being smaller for the softer cartilage). Other more explicit modeling of the extracellular matrix e.g. as another type of (smaller) interacting particle are also thinkable and would be easily realisable within the framework of cell-center based models.

Our model paves the way for future computational studies of cartilage development that may reflect longer durations of bone morphogenesis and thus allow us to simulate the full geometry of embryonic bones until larger structures such as growth plates of the skull are fully formed. In these models, a dynamically changing, rather than fixed, boundary conditions

may be desirable. Our methods may also enable studies of bone morphogenesis in different geometries. Kaucka et al. reported that cartilage contains transversely oriented columns not only in growth plates, which were discussed here, but also in rod-like cartilage that will later turn into digits or ribs. In these tissues, circular transversal structure cross-section of the cartilage contain columns that are slightly bent and have varying lengths. We believe that our presented computational framework for testing verbal hypotheses on cartilage formation may reveal insights into morphogenesis is of long cartilage structures with varying geometries, and how and the corresponding bone structures may be formed robustly. Specifically, how growth is coordinated to achieve correct scaling in the transversal and lateral directions of growth.

The ability to accurately simulate the formation of cartilage and bone in varying geometries will be a crucial step towards advances in tissue engineering. Such simulations may also provide insights into skeletal developmental disorders, such as achondroplasia [44].

Acknowledgments

SM and AH acknowledge funding from the NIH under grant no. NIH/2R01EB014877-04A1 and from the eSSENCE strategic initiatives on eScience. SM acknowledges a travel grant from the Anna-Maria Lundins stipend at Smålands Nation in Uppsala to visit the University of St Andrews. The funders had no role in study design, data collection and analysis, decision to publish, or preparation of the manuscript.

References

[1] M. Kaucka, T. Zikmund, M. Tesarova, D. Gyllborg, A. Hellander, J. Jaros, J. Kaiser, J. Petersen, B. Szarowska, P. T. Newton, V. Dyachuk, L. Li, H. Qian, A.-S. Johansson, Y. Mishina, J. D. Currie, E. M. Tanaka, A. Erickson, A. Dudley, H. Brismar, P. Southam, E. Coen, M. Chen, L. S. Weinstein, A. Hampl, E. Arenas, A. S. Chagin, K. Fried, and I. Adameyko, "Oriented clonal cell dynamics enables accurate growth and shaping of vertebrate cartilage," *eLife*, vol. 6, apr 2017.

[2] J. R. Collier, N. A. Monk, P. K. Maini, and J. H. Lewis, "Pattern Formation by Lateral Inhibition with Feedback: a Mathematical Model of Delta-Notch Intercellular Signalling," *J. Theor. Biol.*, vol. 183, pp. 429–446, dec 1996.

[3] M. Cohen, M. Georgiou, N. L. Stevenson, M. Miodownik, and B. Baum, "Dynamic Filopodia Transmit Intermittent Delta-Notch Signaling to Drive Pattern Refinement during Lateral Inhibition," *Dev. Cell*, vol. 19, no. 1, pp. 78–89, 2010.

[4] S. B. Nissen, M. Perera, J. M. Gonzalez, S. M. Morgani, M. H. Jensen, K. Sneppen, J. M. Brickman, and A. Trusina, "Four simple rules that are sufficient to generate the mammalian blastocyst," *PLoS biology*, vol. 15, no. 7, p. e2000737, 2017.

[5] R. Farhadifar, J.-C. Röper, B. Aigouy, S. Eaton, and F. Jülicher, "The Influence of Cell Mechanics, Cell-Cell Interactions, and Proliferation on Epithelial Packing," *Curr. Biol.*, vol. 17, pp. 2095–2104, dec 2007.

[6] Y. Mao, A. L. Tournier, A. Hoppe, L. Kester, B. J. Thompson, and N. Tapon, "Differential proliferation rates generate patterns of mechanical tension that orient tissue growth," *EMBO J.*, vol. 32, pp. 2790–2803, sep 2013.

[7] J. Metzcar, Y. Wang, R. Heiland, and P. Macklin, "A Review of Cell-Based Computational Modeling in Cancer Biology," *JCO Clin. Cancer Informatics*, pp. 1–13, dec 2019.

[8] A. R. Anderson and M. A. Chaplain, "Continuous and discrete mathematical models of tumor-induced angiogenesis," *Bull. Math. Biol.*, vol. 60, no. 5, pp. 857–899, 1998.

[9] D. Drasdo and S. Hoehme, "A single-cell-based model of tumor growth in vitro: monolayers and spheroids," *Physical Biology*, vol. 2, pp. 133–147, jul 2005.

[10] A. G. Fletcher, M. Osterfield, R. E. Baker, and S. Y. Shvartsman, "Vertex models of epithelial morphogenesis," *Biophysical journal*, vol. 106, no. 11, pp. 2291–2304, 2014.

[11] S. M. Peirce, E. J. Van Gieson, and T. C. Skalak, "Multicellular simulation predicts microvascular patterning and in silico tissue assembly," *The FASEB journal*, vol. 18, no. 6, pp. 731–733, 2004.

[12] F. Graner and J. A. Glazier, "Simulation of biological cell sorting using a two-dimensional extended potts model," *Physical review letters*, vol. 69, no. 13, p. 2013, 1992.

[13] F. R. Cooper, R. E. Baker, M. O. Bernabeu, R. Bordas, L. Bowler, A. Bueno-Orovio, H. M. Byrne, V. Carapella, L. Cardone-Noott, J. Cooper, *et al.*, "Chaste: Cancer, heart and soft tissue environment," *Journal of Open Source Software*, vol. 5, no. 47, p. 1848, 2020.

[14] M. H. Swat, G. L. Thomas, J. M. Belmonte, A. Shirinifard, D. Hmeljak, and J. A. Glazier, "Multi-scale modeling of tissues using compucell3d," in *Computational Methods in Cell Biology* (A. R. Asthagiri and A. P. Arkin, eds.), vol. 110 of *Methods in Cell Biology*, pp. 325–366, Academic Press, 2012.

[15] A. Ghaffarizadeh, R. Heiland, S. H. Friedman, S. M. Mumenthaler, and P. Macklin, "PhysiCell: An open source physics-based cell simulator for 3-d multicellular systems," *PLOS Computational Biology*, vol. 14, p. e1005991, feb 2018.

[16] J. Starruß, W. de Back, L. Brusch, and A. Deutsch, "Morpheus: a user-friendly modeling environment for multiscale and multicellular systems biology," *Bioinformatics*, vol. 30, pp. 1331–1332, 01 2014.

[17] R. J. Lycke, M. K. Walls, and S. Calve, "Computational modeling of developing cartilage using experimentally derived geometries and compressive moduli," *J. Biomech. Eng.*, vol. 141, no. 8, pp. 1–8, 2019.

[18] S. Christley, M. S. Alber, and S. A. Newman, "Patterns of mesenchymal condensation in a multiscale, discrete stochastic model," *PLoS Comput. Biol.*, vol. 3, no. 4, pp. 743–753, 2007.

[19] T. Glimm and J. Zhang, "Numerical Approach to a Nonlocal Advection-Reaction-Diffusion Model of Cartilage Pattern Formation," *Math. Comput. Appl.*, vol. 25, no. 2, p. 36, 2020.

[20] R. Lesage, J. Kerkhofs, and L. Geris, "Computational modeling and reverse engineering to reveal dominant regulatory interactions controlling osteochondral differentiation: Potential for regenerative medicine," *Front. Bioeng. Biotechnol.*, vol. 6, no. NOV, pp. 1–16, 2018.

[21] S. Schivo, S. Khurana, K. Govindaraj, J. Scholma, J. Kerkhofs, L. Zhong, X. Huang, J. van de Pol, R. Langerak, A. J. van Wijnen, L. Geris, M. Karperien, and J. N. Post, "ECHO, the executable CHOndrocyte: A computational model to study articular chondrocytes in health and disease," *Cell. Signal.*, vol. 68, no. June 2018, 2020.

[22] K. M. Márquez-Flórez, J. R. Monaghan, S. J. Shefelbine, A. Ramirez-Martínez, and D. A. Garzón-Alvarado, "A computational model for the joint onset and development," *J. Theor. Biol.*, vol. 454, pp. 345–356, 2018.

[23] N. C. Nowlan, P. Murphy, and P. J. Prendergast, "Mechanobiology of embryonic limb development," *Ann. N. Y. Acad. Sci.*, vol. 1101, pp. 389–411, 2007.

[24] J. J. Vaca-González, M. Moncayo-Donoso, J. M. Guevara, Y. Hata, S. J. Shefelbine, and D. A. Garzón-Alvarado, "Mechanobiological modeling of endochondral ossification: an experimental and computational analysis," *Biomech. Model. Mechanobiol.*, vol. 17, no. 3, pp. 853–875, 2018.

[25] W. Wilson, C. C. Van Donkelaar, R. Van Rietbergen, and R. Huiskes, "The role of computational models in the search for the mechanical behavior and damage mechanisms of articular cartilage," *Med. Eng. Phys.*, vol. 27, no. 10, pp. 810–826, 2005.

[26] J. P. Halloran, S. Sibole, C. C. Van Donkelaar, M. C. Van Turnhout, C. W. Oomens, J. A. Weiss, F. Guilak, and A. Erdemir, "Multiscale mechanics of articular cartilage: Potentials and challenges of coupling musculoskeletal, joint, and microscale computational models," *Ann. Biomed. Eng.*, vol. 40, no. 11, pp. 2456–2474, 2012.

[27] P. Julkunen, W. Wilson, H. Isaksson, J. S. Jurvelin, W. Herzog, and R. K. Korhonen, "A review of the combination of experimental measurements and fibril-reinforced modeling for investigation of articular cartilage and chondrocyte response to loading," *Comput. Math. Methods Med.*, vol. 2013, 2013.

[28] S. M. M. Elhamian, M. Alizadeh, M. M. Shokrieh, and A. Karimi, "A depth dependent transversely isotropic micromechanic model of articular cartilage," *J. Mater. Sci. Mater. Med.*, vol. 26, no. 2, pp. 1–10, 2015.

[29] L. Li and S. Ahsanizadeh, *Computational modelling of articular cartilage*. Elsevier Ltd., 2 ed., 2021.

[30] D. Pearce, S. Fischer, F. Huda, and A. Vahdati, "Applications of Computer Modeling and Simulation in Cartilage Tissue Engineering," *Tissue Eng. Regen. Med.*, vol. 17, no. 1, pp. 1–13, 2020.

[31] F. A. Meineke, C. S. Potten, and M. Loeffler, "Cell migration and organization in the intestinal crypt using a lattice-free model," *Cell Proliferation*, vol. 34, pp. 253–266, aug 2001.

[32] A. DeLise, L. Fischer, and R. Tuan, "Cellular interactions and signaling in cartilage development," *Osteoarthritis and Cartilage*, vol. 8, pp. 309–334, sep 2000.

[33] E. M. Purcell, "Life at low reynolds number," *American Journal of Physics*, vol. 45, pp. 3–11, jan 1977.

[34] M. B. Goldring, K. Tsuchimochi, and K. Ijiri, "The control of chondrogenesis," *Journal of Cellular Biochemistry*, vol. 97, no. 1, pp. 33–44, 2005.

[35] B. K. Hall and T. Miyake, "All for one and one for all: condensations and the initiation of skeletal development," *BioEssays*, vol. 22, pp. 138–147, jan 2000.

[36] D. F. Griffiths and D. J. Higham, *Numerical methods for ordinary differential equations: initial value problems*. London: Springer Science & Business Media, 2010.

[37] F. Long and T. F. Linsenmayer, "Regulation of growth region cartilage proliferation and differentiation by perichondrium," *Development*, vol. 125, no. 6, pp. 1067–1073, 1998.

[38] H. M. Kronenberg, "The role of the perichondrium in fetal bone development," *Annals of the New York Academy of Sciences*, vol. 1116, no. 1, pp. 59–64, 2007.

[39] C. Colnot, C. Lu, D. Hu, and J. A. Helms, "Distinguishing the contributions of the perichondrium, cartilage, and vascular endothelium to skeletal development," *Developmental biology*, vol. 269, no. 1, pp. 55–69, 2004.

[40] D. Gvaramia, J. Kern, Y. Jakob, M. Zenobi-Wong, and N. Rotter, "Regenerative potential of perichondrium: A tissue engineering perspective," *Tissue Engineering Part B: Reviews*, 2021.

[41] J. Delile, M. Herrmann, N. Peyriéras, and R. Doursat, "A cell-based computational model of early embryogenesis coupling mechanical behaviour and gene regulation," *Nature Communications*, vol. 8, p. 13929, jan 2017.

[42] S. Mathias, A. Coulier, A. Bouchnita, and A. Hellander, "Impact of force function formulations on the numerical simulation of centre-based models," *Bull. Math. Biol.*, vol. 82, p. 132, 2020.

[43] B. K. Hall, "Chapter 1 - vertebrate skeletal tissues," in *Bones and Cartilage (Second Edition)* (B. K. Hall, ed.), pp. 3–16, San Diego: Academic Press, second edition ed., 2015.

[44] G. Baujat, L. Legeai-Mallet, G. Finidori, V. Cormier-Daire, and M. Le Merrer, "Achondroplasia," *Best Practice & Research Clinical Rheumatology*, vol. 22, no. 1, pp. 3–18, 2008. Orphan Skeletal Diseases.